

## **Chapter 20. Synthetic Aperture Radar for Operational Ice Observation and Analysis at the U.S., Canadian, and Danish National Ice Centers**

**Cheryl Bertoia**

U.S. National Ice Center, Washington D.C. USA

**Michael Manore**

Canadian Ice Service, Environment Canada, Ottawa, Ontario, Canada

**Henrik Steen Andersen**

Danish Meteorological Institute, Copenhagen, Denmark

**Chris O’Connors**

U.S. National Ice Center, Washington D.C. USA

**Keld Q. Hansen**

Danish Meteorological Institute, Copenhagen, Denmark

**Craig Evanego**

U.S. National Ice Center, Washington D.C. USA

### **20.1 Operational Ice Services**

Operational ice services from more than a dozen nations routinely issue ice and iceberg bulletins, warnings, analysis charts, and forecasts to support safe navigation in ice-affected waters. In addition, these ice analysis products are increasingly being used as a record of ice conditions to support climate change studies.

Operational ice services from the major ice charting nations of the Arctic (Figure 20.1) work in remarkably similar manners, but with differences in their geographic regions of interest, user base, and analysis data sets. Most centers now rely heavily on satellite image data as a primary data source, supplemented by airborne reconnaissance (visual or with imaging radar), ship reports, and meteorological and oceanographic inputs. Ice is highly dynamic and requires frequent and timely data sources for accurate charting. Each operational ice center has invested in the infrastructure to receive, analyze, and disseminate large volumes of data in near-real-time. Virtually all data is now processed in digital form and geographic information systems are used to create and disseminate products.

This chapter addresses work at the U.S., Canadian, and Danish national ice services; information specific to other ice services can be found in World Meteorological Organization Publication No 574 (available at [http://www.aari.nw.ru/gdsidb/gdsidb\\_2.html](http://www.aari.nw.ru/gdsidb/gdsidb_2.html)).

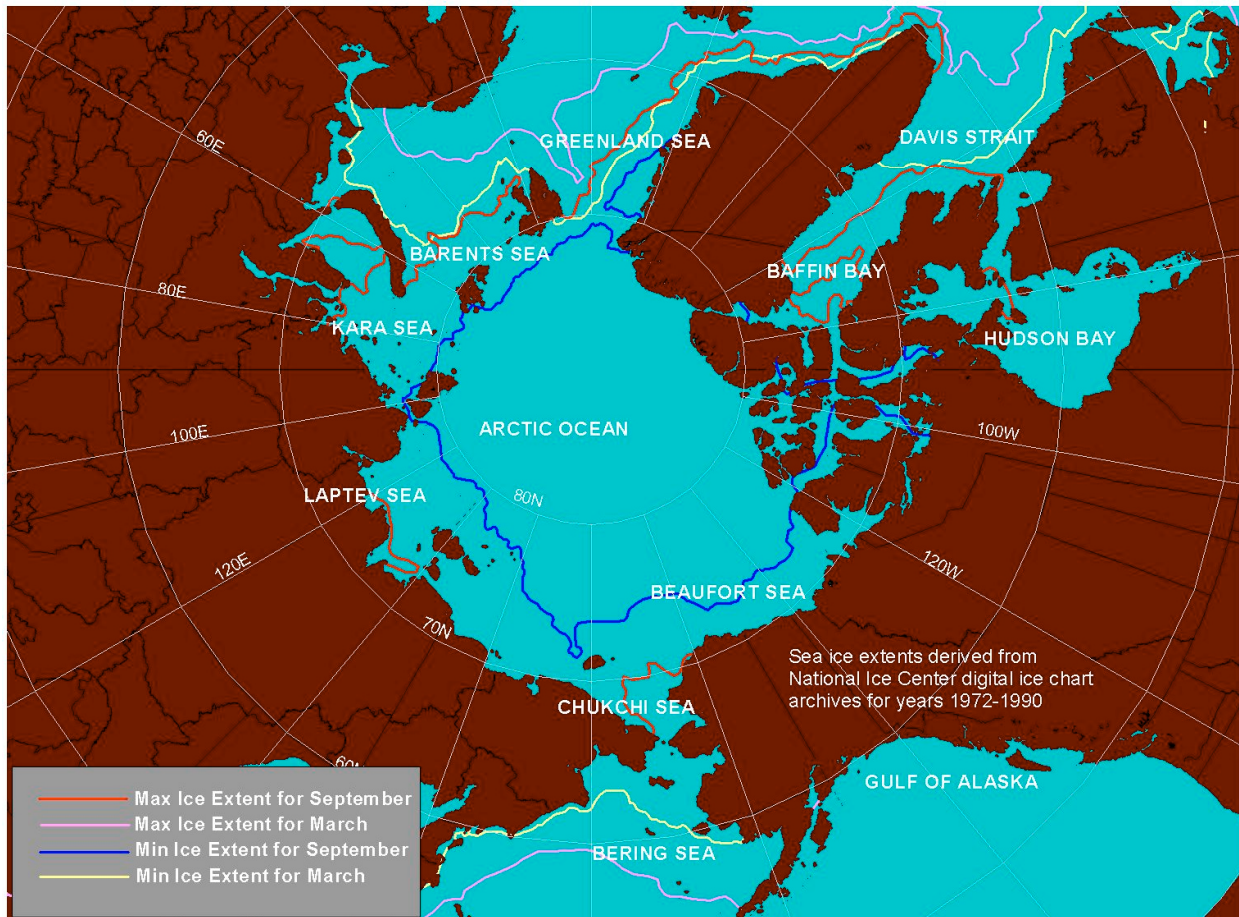


Figure 20.1. Northern Hemisphere climatological sea ice extent, based on U.S. National Ice Center data from 1972 to 1994. The complete data set is available from the National Snow and Ice Data Center in Boulder, Colorado.

## 20.2 Satellite Data Sources

The National Oceanic and Atmospheric Administration (NOAA) Advanced Very High Resolution Radiometer (AVHRR) sensor, originally developed for meteorological applications but well suited to ice monitoring, has been a long-standing workhorse for many ice centers because of its ready availability and frequent coverage. The AVHRR produces visible and thermal imagery: in addition to its optical channels, the thermal bands permit imaging of ice and interpretation of ice thickness, even in periods of polar darkness. Its 1-km resolution permits the charting of strategic ice information suitable for making general ship routing recommendations, but not for close tactical navigation. Other nations use equivalent meteorological satellites such as Japan's GMS or Russia's Meteor systems. The U.S. National Ice Center (NIC) also makes extensive use the Operational Linescan System (OLS) from the Defense Meteorological Satellite Program (DMSP) satellites, which provide 0.5 km visible and thermal imagery. Of course, the main limitation of optical systems is their susceptibility to cloud cover. Cloud cover or fog typically obscures the part of the ice pack of greatest interest to ship traffic—the area near the ice edge—about 70% of the time.

Ice services also rely on passive microwave imagery from the Special Sensor Microwave/Imager (SSM/I) sensor on the U.S. DMSP satellites to provide near daily, all weather, multi-channel microwave radiometry over a 1394-km swath. Automatic algorithms for the extraction of ice edge, total ice concentration, and multi-year ice concentration have been developed and validated over many years. There are probably a dozen or more global algorithms or regionally-tuned variants running on an operational or semi-operational basis worldwide, each with specific advantages or limitations in resolution, atmospheric attenuation, sensitivity to low concentrations, regional ice types, etc. In all cases, the SSM/I sensor provides only relatively coarse resolution (12.5 km to 25 km) sea ice products, but it is a reliable data source for regions where only basic ice edge and ice concentration information is required for strategic navigation decisions, such as Antarctica. In addition, the relatively long record of passive microwave data (1972 to present) and the coarse resolution make it a favored data source for ice-related climate change studies at hemispheric scales.

Because of weather, polar darkness, and the desire for higher resolution imagery, the ice services have had a strong interest in radar remote sensing since the technology emerged [Bertoia *et al.*, 1998]. As far back as the early 1970s, airborne real aperture radars (RARs) were used to map the ice pack and, in the 1980s and 1990s, airborne Synthetic Aperture Radar (SAR) and RAR systems were in operational use. In 1991, the European Space Agency's ERS-1 provided the first sustained taste of satellite radar data and, in 1996, wide-swath (500 km) SAR data became available from the Canadian Space Agency's RADARSAT-1. SAR data offers the advantage of high-resolution imaging through clouds and polar darkness, and sensitivity to the surface roughness and salinity properties of sea ice that help to distinguish different ice types (see Chapter 3). RADARSAT-1 data was quickly adopted by the Canadian and U.S. ice services under national data allocations, and later by several European ice services on a commercial basis. At the Danish Meteorological Institute (DMI) and at other centers, the purchase of satellite SAR imagery has been made possible through cost savings by reducing or eliminating aircraft reconnaissance. RADARSAT-1 has been used in demonstration projects for ice monitoring in Russia, Japan, and China, but its use has not yet been adopted operationally. It is estimated that more than 10,000 scenes per year of SAR data are currently used for operational ice monitoring.

Recent and future multi-polarization SAR systems (ENVISAT, ALOS, and RADARSAT-2) are expected to improve the quality of ice information available from SAR imagery. However, these systems will also increase data volume and place additional demands on processing and communications systems needed to meet the near-real-time image delivery requirement of the ice services. In addition, new analysis techniques must be developed for multi-polarization and fully polarimetric data in order for this data to be included in the operational processing flow. Ice centers expect to combine data from these multiple SAR sources in order to resolve ambiguities in ice type discrimination that can occur when using only single frequency and polarization SAR data. Other work includes improvements in image processing approaches to detect low concentrations of sea ice and improved detection of icebergs. The operational centers look forward to a constellation of SAR satellites that will permit better spatial and temporal coverage, as well as provide operational redundancy in the event of system failure.

### 20.3 Case Studies

The following case studies present examples of how ice centers have used SAR data to provide navigational support and to create ice maps in conjunction with other data sources.

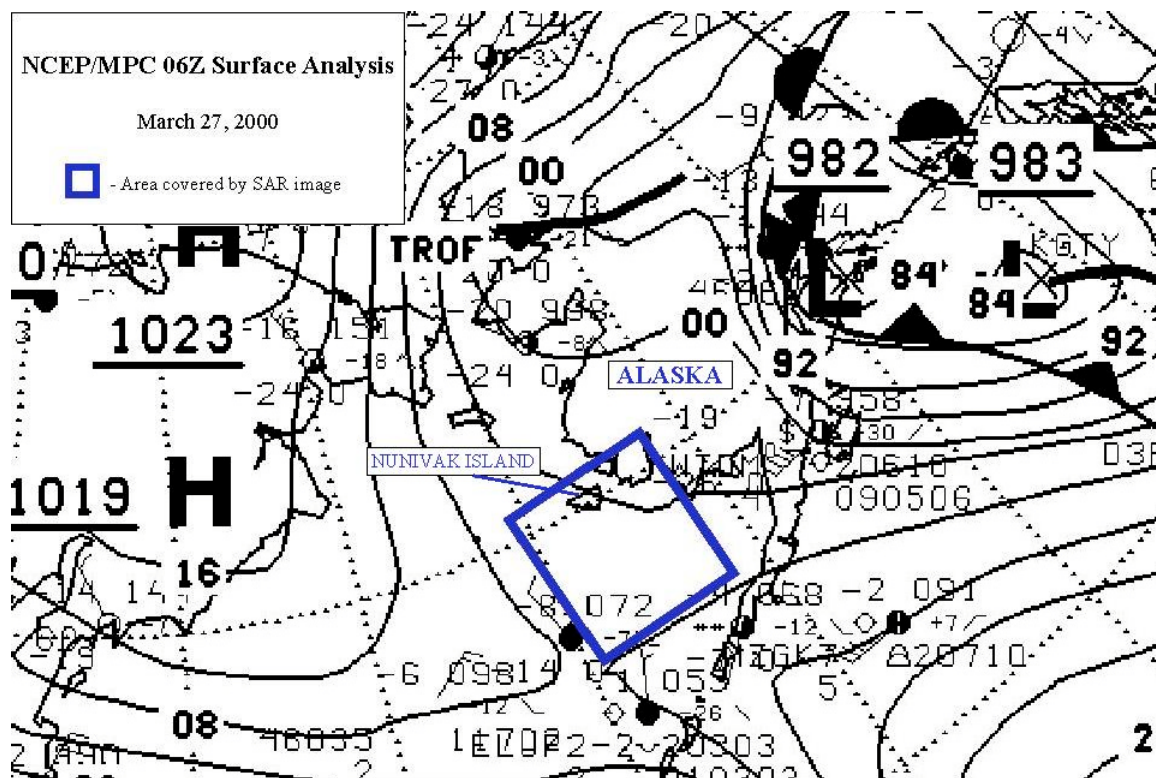


Figure 20.2. NCEP 0600 UTC Surface analysis valid for 27 March 2000 covering the Bering Sea. Strong pressure gradient north of the highlighted box (in blue), which corresponds with RADARSAT-1 images (Figure 20.4), corroborates the strong northwesterly winds observed on the satellite imagery (Figure 20.3).

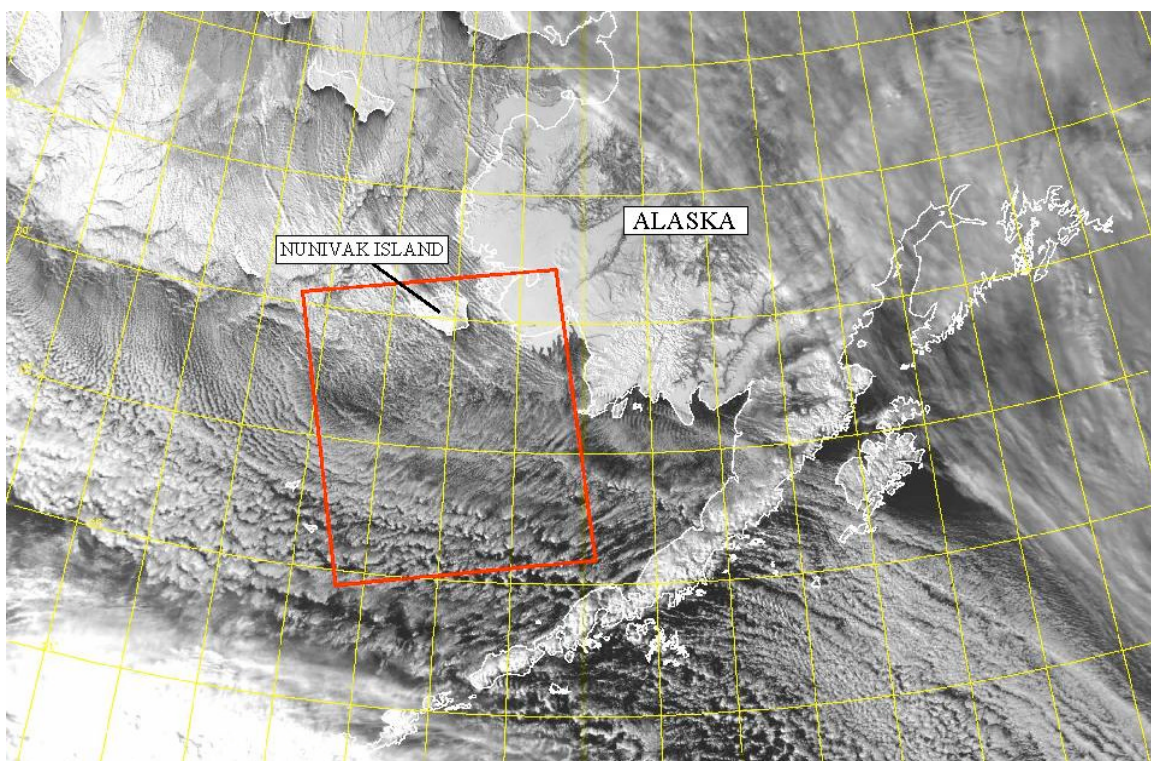


Figure 20.3. NOAA Advanced Very High-Resolution Radiometer (AVHRR) visible image from 0144 UTC on 27 March 2000. The red box shows the approximate position of the RADARSAT-1 SAR image in Figure 20.4.

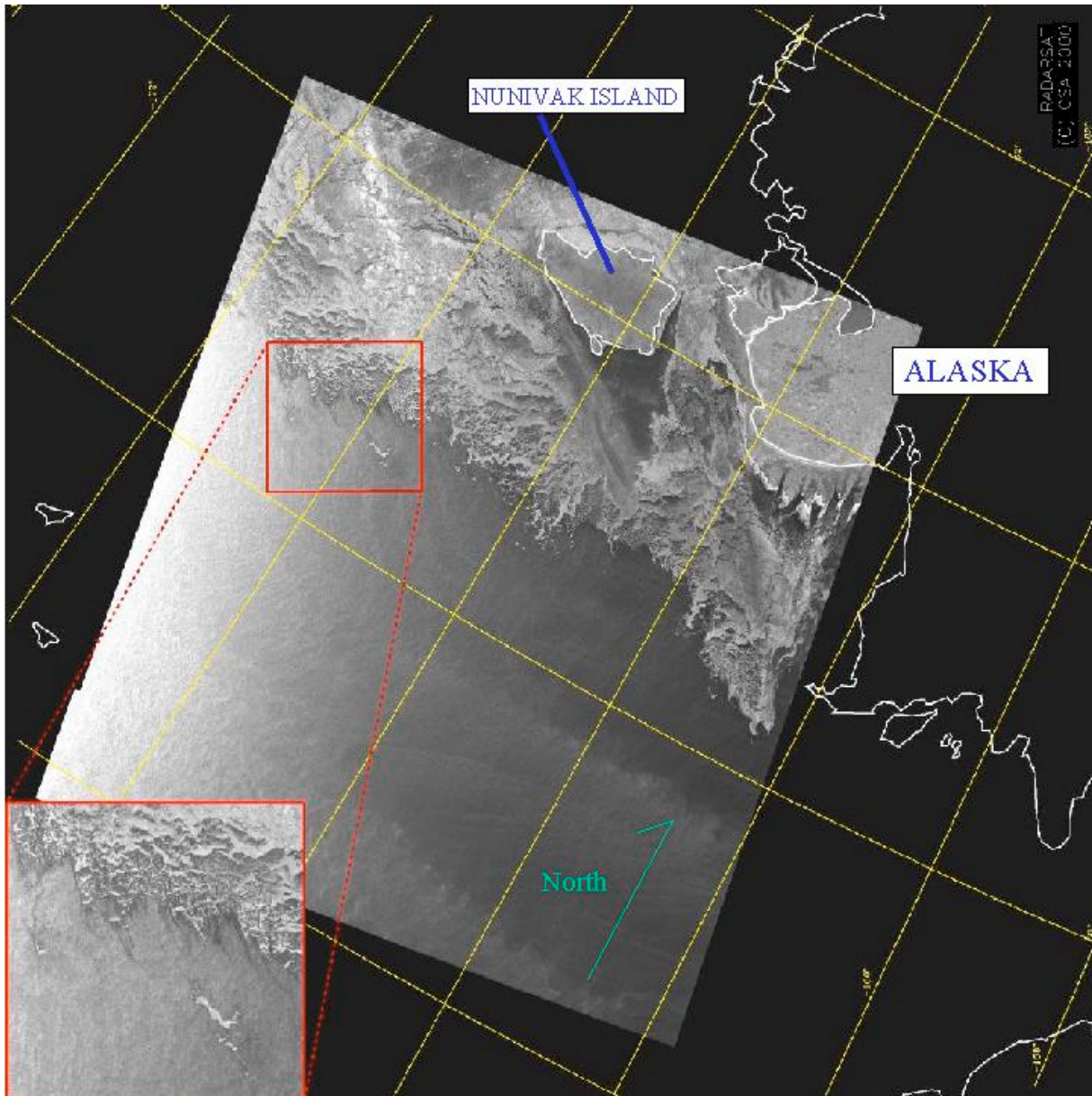


Figure 20.4. RADARSAT-1 (C-band, HH) ScanSAR Wide image acquired at 0442 UTC on 27 March 2000. The zoom box shows fine belts and strips of ice near the edge. NIC's SAR imagery is processed to 100-m pixels, and then averaged to 500-m pixel spacing, making the detection of these small features possible, while eliminating classification confusion caused by image speckle. ©CSA 2000

### 20.3.1 U.S. National Ice Center: Bering Sea Analysis, 27 March 2000

Working under Navy, NOAA, and Coast Guard sponsorship, the U.S. National Ice Center (NIC) produces a suite of global sea ice charts including twice-weekly charts of the Alaskan region (available at <http://www.natice.noaa.gov>) in support of shipping and fisheries operations and other national interests in the Bering, Beaufort, and Chukchi Seas. To create the Alaskan ice maps, the NIC receives approximately 5000 RADARSAT-1 ScanSAR Wide B SAR images per year from the Alaska SAR Facility (ASF) in Fairbanks, Alaska. Each image is typically received at the NIC less than three hours after the image is acquired at ASF.

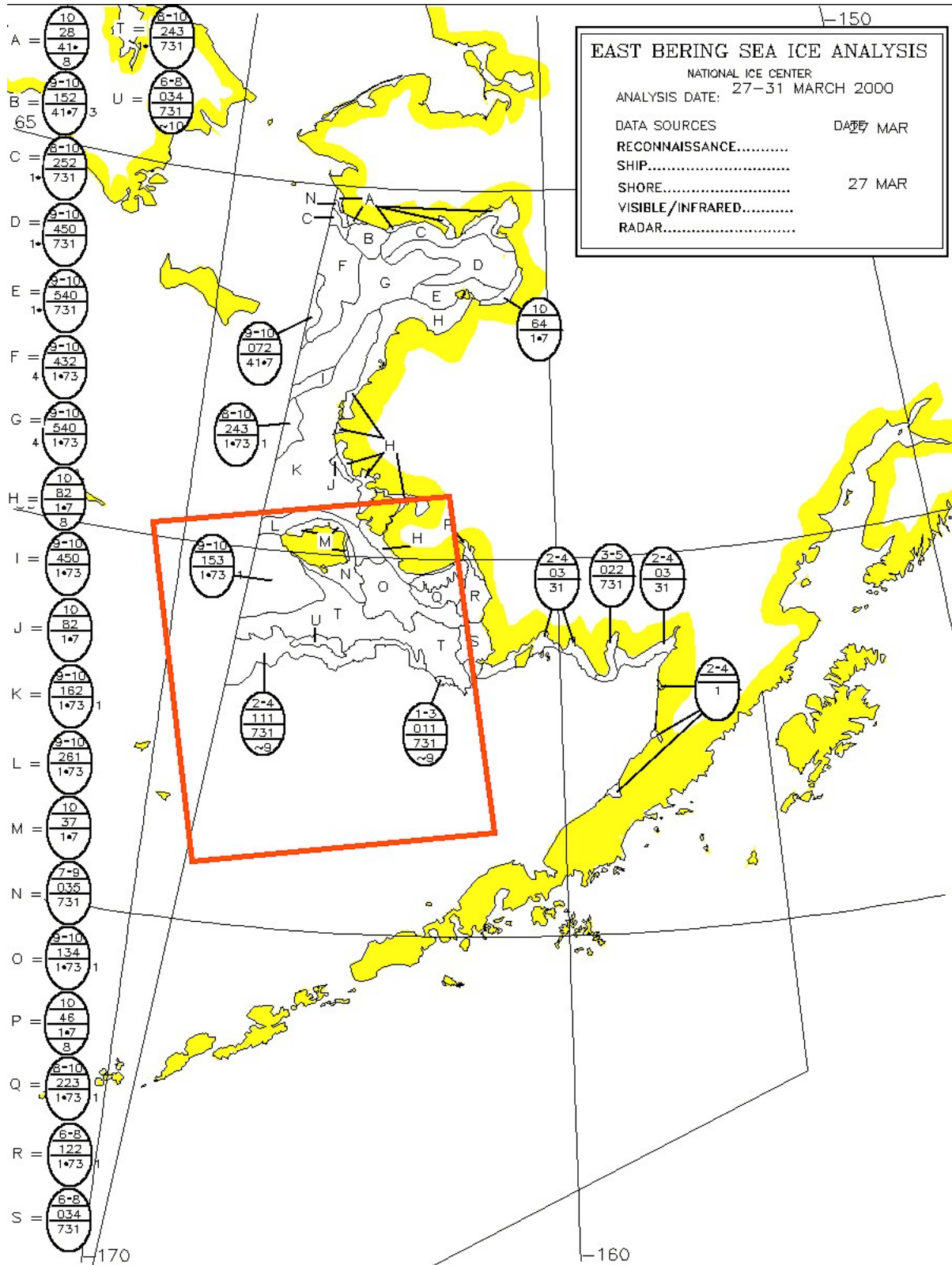


Figure 20.5. NIC Alaskan regional sea ice analysis chart for 27 March 2000. Sea ice total concentration and ice type (a proxy for ice thickness) are encoded using the World Meteorological Organization’s “egg code” (fully described in the ice chart symbology section at the end of the chapter).

On 27 March 2000, a National Centers for Environmental Prediction (NCEP) surface analysis (Figure 20.2) showed northwesterly winds generated by the circulation around a storm system over southeastern Alaska flowing over the eastern Bering Sea. These winds dragged cold (less than 0°C) air across the ice pack and out over the relatively warm open water in the southern Bering Sea. The cold air streaking over the open water produced bands of stratocumulus clouds, obscuring the marginal ice zone and ice edge. Clearing skies behind the storm system allowed good visibility of the inner ice pack on the visible AVHRR image (Figure 20.3). Visible and infrared imagery from NOAA satellites is a useful adjunct to SAR imagery, providing valuable clues to ice type/thickness.

A coincident RADARSAT-1 image (Figure 20.4) shows belting and stripping of new, young, and first-year ice along the Marginal Ice Zone (MIZ). The MIZ is the region of the ice pack adjacent to and affected by the open sea and is an area of enhanced ice drift, deformation, and divergence. Most shipping operates in or near the MIZ and, thus, operational ice centers concentrate on mapping this area in fine detail. Though in this case the MIZ and the ice edge are obscured by streaks of stratocumulus clouds, the RADARSAT-1 image allowed the ice analyst to accurately analyze the ice edge and marginal ice zone for the NIC weekly ice analysis (Figure 20.5).

Accurate depiction of the ice edge is particularly important to the large Alaskan snow crab industry in the Bering Sea. Crab fishermen typically set traps in the vicinity of the ice edge, and thus require a detailed analysis of changes in extent at or near the ice edge for safety of operations. Clouds often obscure the marginal ice zone and ice edge during the Alaskan winter for months at a time. SAR's ability to see through clouds and provide images day or night makes it a crucial resource for safety of lives and property in the Alaskan crab and fishing fleets. This case study represents typical weather and ice conditions in the Bering Sea during the winter.

NIC has been incorporating SAR image analysis into operational sea ice charts since ERS-1 data became routinely available in 1992. Analysts have found SAR imagery irreplaceable for analyzing ice concentrations and determining ice types, particularly in the MIZ and along the often cloud-obscured ice edge. SAR imagery has proven to be an excellent tool for detecting new ice, which is nearly impossible to detect with other routinely available, remotely sensed data sources.

### 20.3.2 Canadian Ice Service:

*Canadian Archipelago 1-4 February 2001 and 12 May 1999-30 June 1999*

The region of the Canadian Arctic islands hosts a diversity of ice regimes composed of multi-year, first-year, and new ice types, as well as icebergs. Ice growth typically starts in late September and continues throughout the Arctic winter until early melt begins in May and June. The extremely cold (-30°C to -40°C) wintertime conditions support rapid and thick sea ice growth. First-year ice will reach a thickness of between 1.5 m and 2.0 m, while multi-year ice may achieve a thickness of 5 m or more. Navigation in this region is limited to the brief Arctic shipping season (July to October) when the ice is weaker because of melt and decay and some areas of open water (leads) are present. Hard, thick multi-year ice poses the greatest hazard to ships' operation in this region, so its detection and mapping is particularly important.

Figure 20.6 is a mosaic of multiple RADARSAT-1 orbits collected 1-4 February 2001. Figure 20.7 is the resulting ice analysis chart derived from the mosaic and published in the Canadian Ice Service's annual Arctic Ice Atlas. The imagery illustrates typical wintertime, cold-

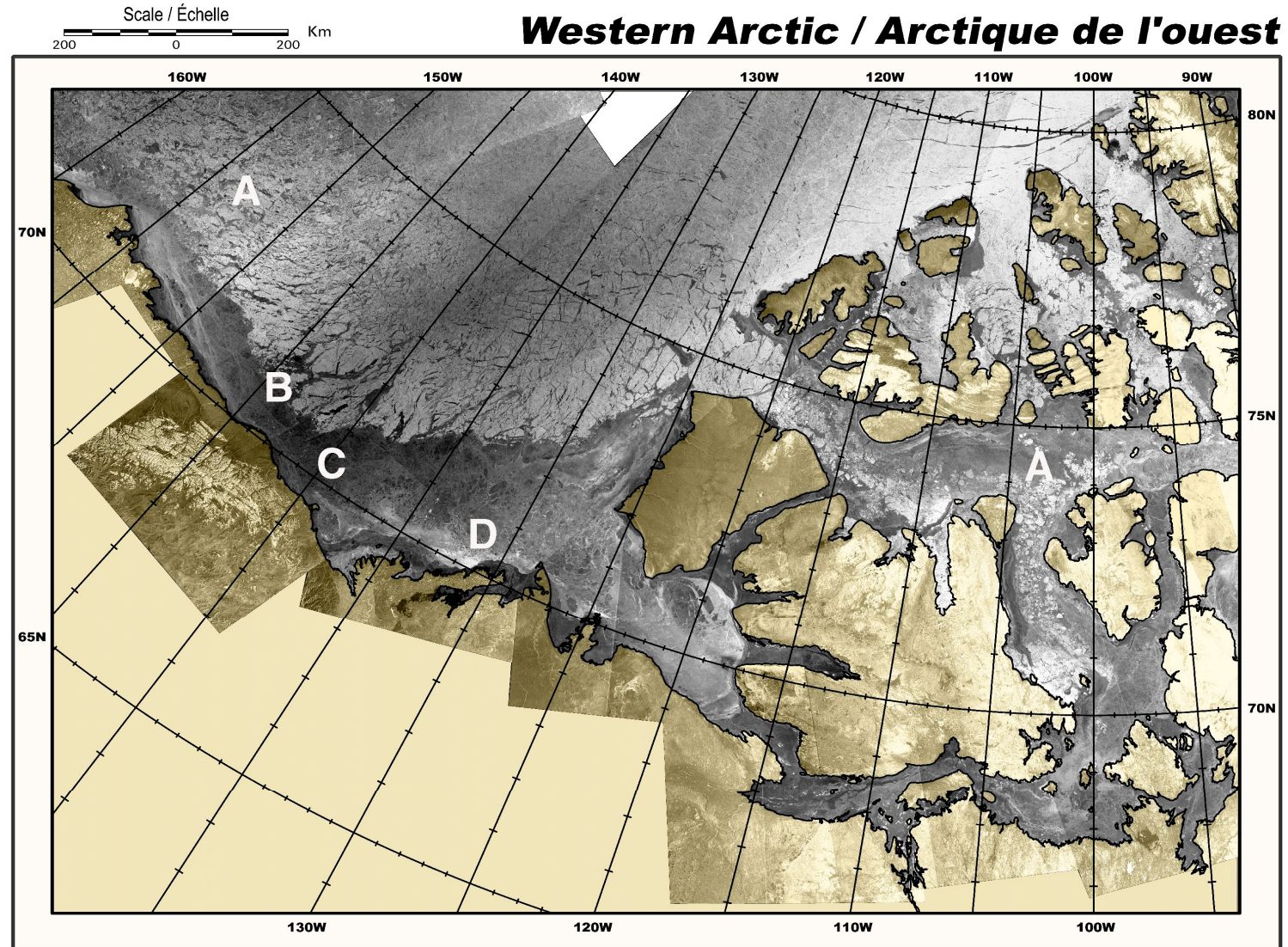


Figure 20.6. Mosaic of RADARSAT-1 (C-band, HH) ScanSAR-Wide imagery, 1-4 February 2001. Imagery from RADARSAT-1 is used operationally by the Canadian Ice Service for daily mapping of ice conditions in areas of active navigation, as well as for an annual Arctic Ice Atlas [see Ramsay *et al.*, 2001] © CSA, 2001

# SAR for Operational Ice Observation and Analysis

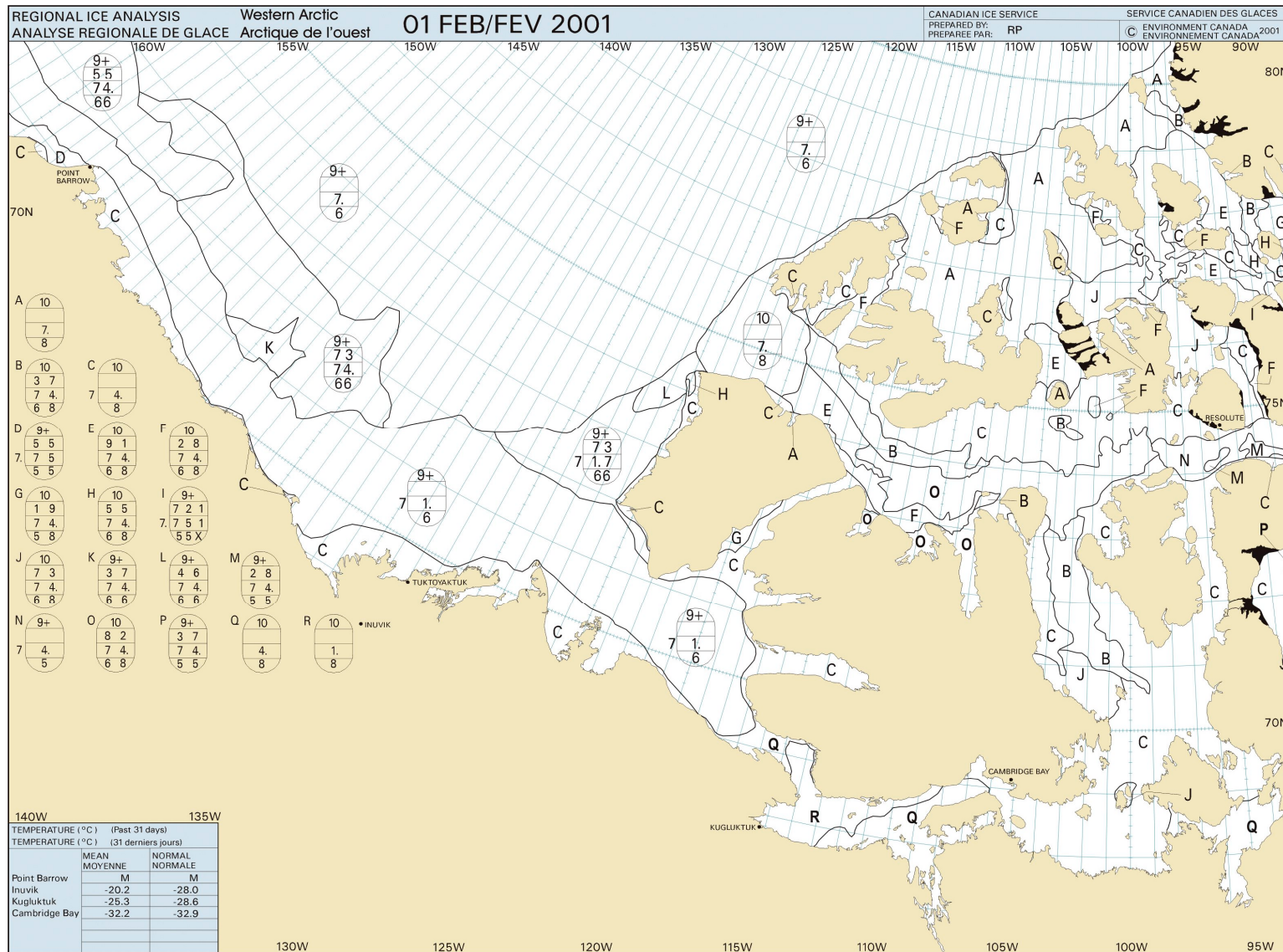


Figure 20.7. Regional Ice Analysis Chart derived from the imagery in Figure 20.6. A series of seven regional charts are produced each year for the Winter Ice Atlas [see Canadian Ice Service, 2001]. This is in addition to the several thousand charts and text bulletins issued every year in areas of active navigation in ice in Canadian waters.

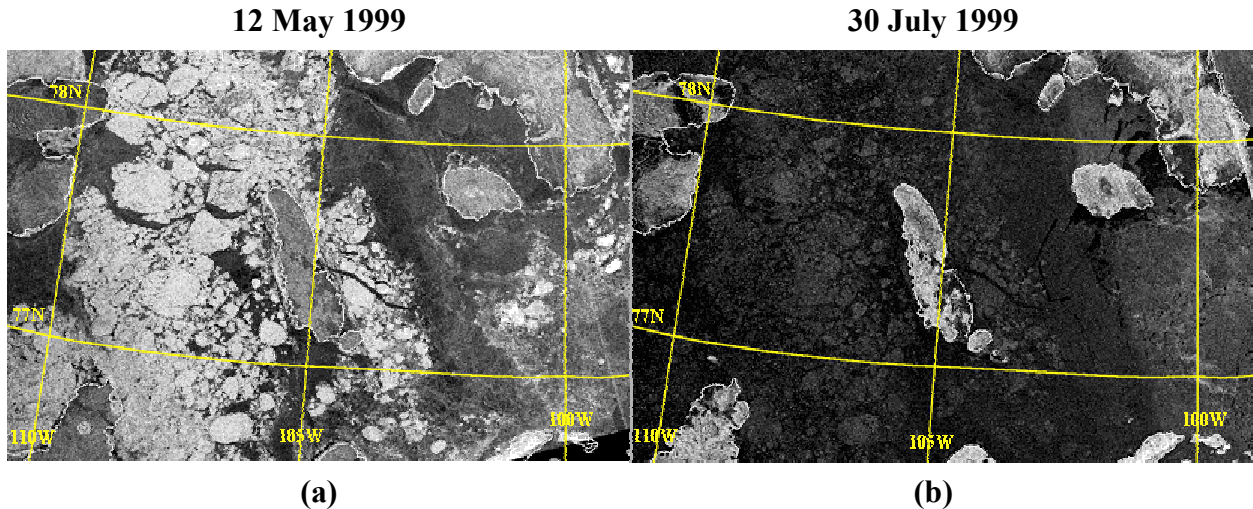


Figure 20.8. Comparison of winter (a) and summer (b) signatures of ice in the Canadian Arctic islands. The contrast in signature between ice types is significantly reduced during the melt season because of the presence of liquid water on the surface of the ice and in the overlying snow pack. ©CSA 1999

weather ice signatures. In Figure 20.6, multi-year ice floes are clearly distinguishable by their bright signature, rounded shape and mottled texture (A). The edge of the multi-year pack ice in the Beaufort Sea is clearly visible in contrast to the seasonal ice along the Yukon, Northwest Territories, and Alaska shores (B). Undeformed first-year ice is dark in tone because of specular reflection from its saline (lossy), smooth surface (C). Deformed ice has a bright signature caused by high surface roughness and multi-bounce scattering (D). Cold, fresh water snow overlaying the ice is virtually transparent at C-band so all returns are controlled by the surface (first-year) or volume (multi-year) scattering characteristics of the underlying ice.

Figures 20.8a and 20.8b are sub-scenes of RADARSAT-1 images around Lougheed Island in the central Arctic islands (77.5°N, 105°W). Figure 20.8a was acquired 12 May 1999 under cold winter conditions and exhibits signatures similar to those in Figure 20.6. Figure 20.8b, however, was acquired 30 July 1999 and illustrates the radical signature change that occurs under wet snow conditions during the melt season. In the summer, the overlying snow pack becomes saturated with liquid water and becomes the main contributor to scattering (and absorption) with the result of masking the returns from ice below. This has the effect of significantly decreasing the contrast between ice types and causing difficulties in interpretation. Multi-year ice that was easily interpreted under cold conditions is now difficult to distinguish from the surrounding first-year ice. As most navigation in the Arctic takes place during the summer, this poses a significant operational challenge. In regions with no or little ice motion, winter imagery is often used in combination with current imagery to aid in multi-year ice detection and avoidance.

Daily and weekly ice analysis charts and bulletins for Canadian waters are available online at <http://ice-glaces.ec.gc.ca>.

### 20.3.3 Danish Meteorological Institute: 12 May 2000

The Danish Meteorological Institute produces satellite-based ice charts for Greenland waters (Figure 20.9) on a routine basis for safety of ship navigation. Recent information about the operational practices and the methods applied by the Danish Meteorological Institute for

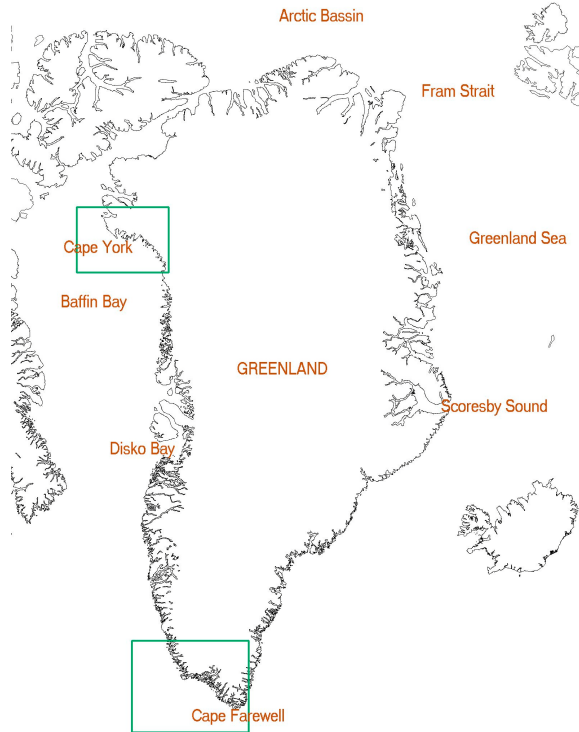


Figure 20.9. Map of the Greenland waters. The green boxes show the areas discussed in sections 20.3.3 and 20.3.4.

operational SAR-based sea ice charting may be found in *Gill, et al.* [2000] and *Gill* [2001]. The area around Greenland is charted for navigation as required by shipping traffic, which means that the east and the northwestern parts of Greenland are mapped during periods of ice formation and break up. The Cape Farewell area is charted several times weekly throughout the year because almost all ships traveling to and from Greenland pass through this area.

The waters off the southernmost part of Greenland—the Cape Farewell area—are some of the world’s most hazardous to navigate because of the combination of frequent severe storms, low visibility, multi-year sea ice, and icebergs. Sea ice is present in this area from December to August, but icebergs originating from the Greenland east coast glaciers occur throughout the year. The distribution of sea ice in the Cape Farewell area is strongly affected by the position and intensity of weather systems and large variations on short time scales may result. In general, sea ice drift is on the order of  $1 \text{ km hr}^{-1}$ , however, higher drift speeds frequently occur.

Sea ice several meters thick drifts to the East Greenland shores from the Arctic Basin via the Fram Strait. This multi-year ice combines with locally-formed first year ice and icebergs in the East Greenland Current as it reaches the Cape Farewell area, then continues around the southern tip of Greenland. The multi-year ice pack often drifts several hundred kilometers north along the west coast of Greenland during the months April through July.

Ice floes in the Fram Strait are often 50 km across or larger. During their southward drift along the Greenland coast, the floes break into smaller pieces and are mixed with first year sea ice, particularly at the ice edge. South of Scoresby Sound the floe sizes seldom exceed 5 km. By the time the ice reaches the Cape Farewell area the floe sizes are usually less than 100 m. These very small floes are mostly multi-year floes with a thickness greater than 2 m and, thus, are a great danger to shipping, even when the ice concentrations are very low or the floe size is only a few meters.

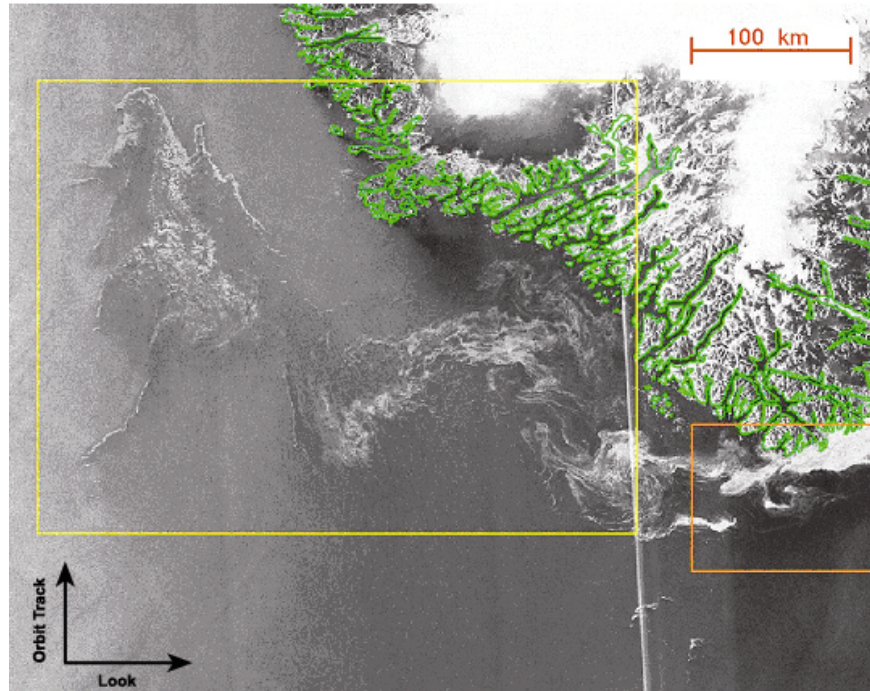


Figure 20.10. A RADARSAT-1 (C-band, HH) ScanSAR Wide scene from 12 May 2000, 2048 UTC covering part of the Cape Farewell area. The pixel size is 100 m. The satellite orbit is ascending and consequently the left part of the image is in near range and the far range is to the right. Often the far range part of the image provides better possibilities for discrimination between sea ice and open sea. The seams between individual beams of the ScanSAR mode are clearly visible going from the top the bottom. The bright line parallel to the beam seams is a nadir ambiguity, a characteristic artifact of this particular ScanSAR mode . ©CSA 2000

The backscatter signatures from open water and sea ice in this region are not unique and it can be very hard (or impossible) to distinguish between these signatures. The backscatter from the water is dominated by the local wind conditions. Backscatter from the ice depends on ice type, ice concentration, surface roughness of the individual floes, and level of surface melting. The backscatter signals are also critically dependent on the radar incident angles. For example, it is quite common that belts of ice appear nearly white in the far range (high incident angle;  $> 40^\circ$ ) and nearly black in the near range (low incident angle;  $< 35^\circ$ ) when viewed against the background sea clutter.

The case from 12 May 2000 represents a typical situation during the Cape Farewell sea ice season. Figures 20.10 to 20.14 present the situation from an ice analyst's point of view. Subsections show details both in the near (Figure 20.11) and far (Figure 20.12) range part of the image and provide examples of wind induced effects and a range of ice concentrations. The resulting analysis and chart are shown in Figures 20.13 and 20.14, respectively. To an experienced ice analyst, the available RADARSAT-1 ScanSAR Wide image is straightforward to interpret. This ease of interpretation may leave the impression that SAR imagery is the ultimate ice-charting tool for ice services and indeed this is true in many cases. However in some cases SAR imagery is extremely difficult to analyze, especially late in the melt season when ice information content drops dramatically. Interpretation is particularly difficult in the case of low concentration multi-year sea ice covered with surface melt water occurring in the near range of the image. Detection of multi-year ice under these conditions is a challenge for the ice analyst as well as for the ice detection algorithms.

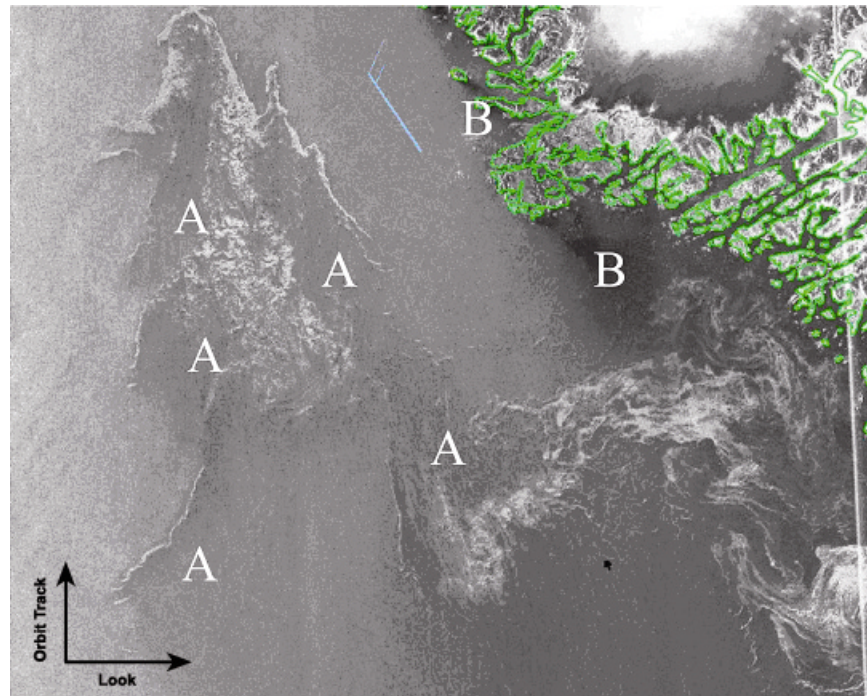


Figure 20.11. A subsection of the image shown in Figure 20.10 (yellow box). The sea surface roughness may be dampened as a consequence of calm winds or the presence of sea ice. Consequently the backscatter signal is reduced. In the areas marked (A), the dampening effect of smooth seas can be seen because of the presence of 10% to 30% sea ice. The wind arrow indicates the northwest direction of the wind ( $7 \text{ m s}^{-1}$  to  $8 \text{ m s}^{-1}$ ) and in area (B) lee effects are clearly visible. ©CSA 2000

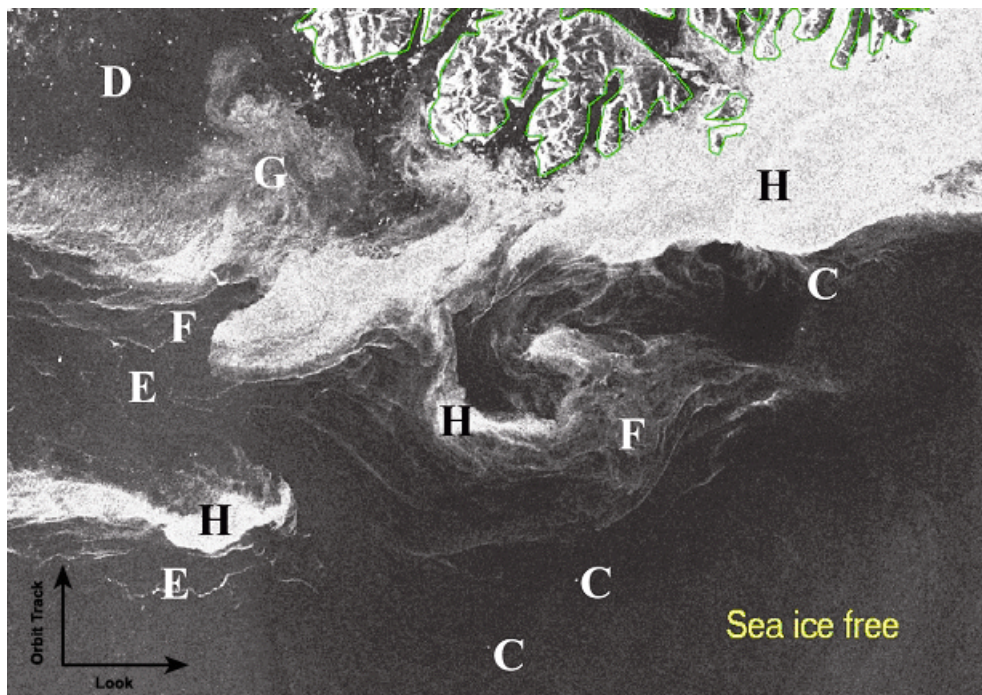


Figure 20.12. A subsection of the image shown in Figure 20.10 (green box). This image illustrates different sea ice concentration levels. In all cases, the sea ice type is predominately multi-year ice with floe sizes ranging from 10 m to 100 m. (C) Icebergs, (D) Icebergs and less than 10% sea ice, (E) less than 10% sea ice, (F) from 10% to 30% sea ice in belts and strips, (G) 40% to 60% sea ice, (H) 90 to 100% sea ice. ©CSA 2000

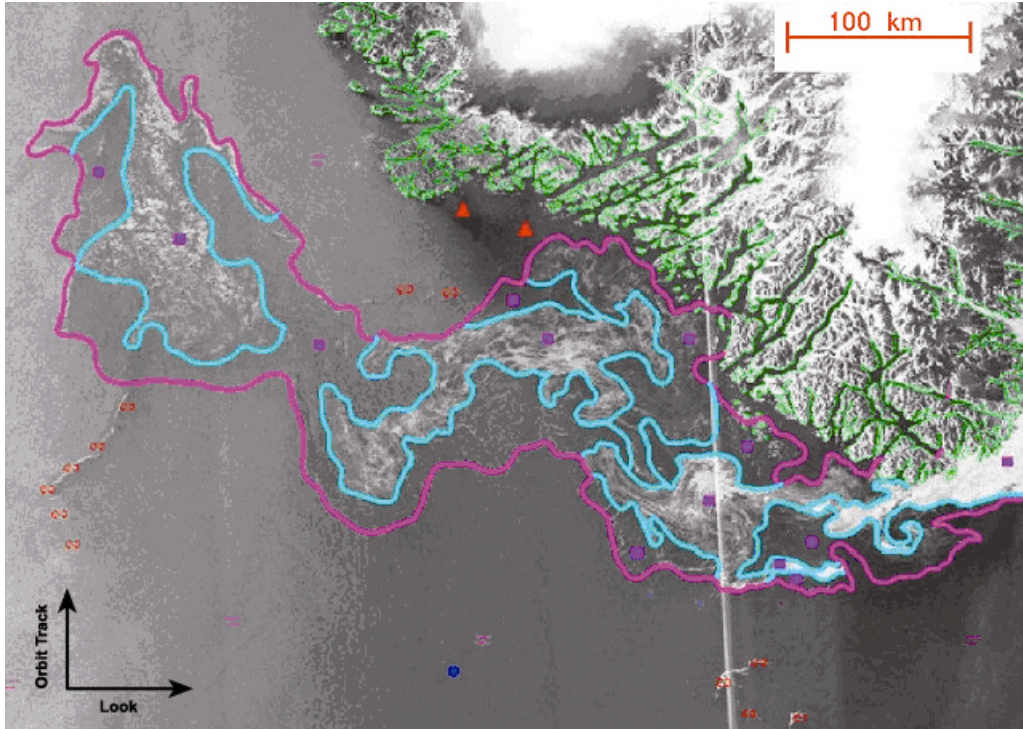


Figure 20.13. The ice analysis resulting from visual interpretation. The ice analyst always tries to generalize the information available in the image to produce a simple yet accurate chart that can be used for navigation. The ice edge is in magenta and the inner boundaries are in cyan. The special symbols indicate the presence of icebergs and belts of ice. ©CSA 2000

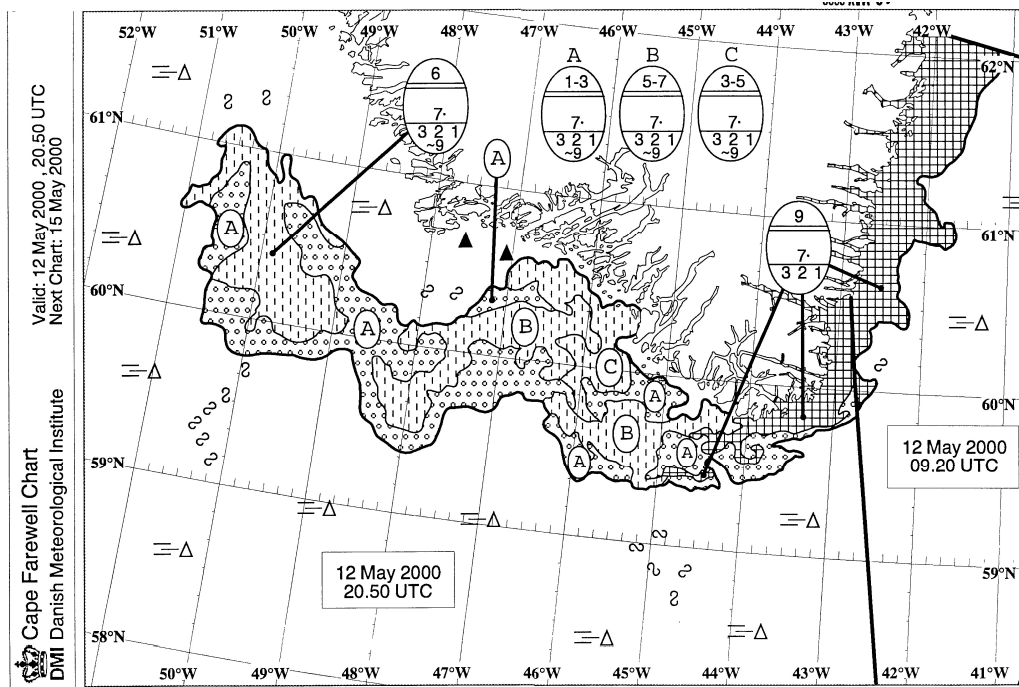


Figure 20.14. The resulting ice chart based on the ice analysis. On an annual basis, DMI produces, in near-real-time, about 180 navigational ice charts for the Cape Farewell waters and about 150 charts for ships operating along the west and east coast of Greenland. Once a week an ice analysis covering all Greenland waters is produced based on all available satellite data and ancillary background information.

### 20.3.4 Operational satellite-based mapping of icebergs at DMI: 27 July 2001

The main problem with using SAR images in the operational mapping of sea ice in the South Greenland waters is that, in many cases, one cannot discriminate between regions of open water and ice. This difficulty is due to the large variability of the backscatter from these regions and the occurrence of very small floes and low ice concentrations. Two methods, the Power-to-Mean-Ratio method (PMR) and The Constant False Alarm Rate method (CFAR), are used operationally at DMI on SAR imagery to obtain and improve information about ice edges and the position of icebergs.

The Power-to-Mean-Ratio is a statistical parameter that helps identify the presence of targets that differ in brightness from the surrounding background. The values of the PMR are computed using a moving window of 20 x 20 pixels and 4 x 4 pixels for inter-window spacing [Gill *et al.*, 1997]. The problem of detecting icebergs in SAR images consists mainly of distinguishing point targets from the background sea clutter and reducing the occurrence of ‘false alarms’. In the CFAR method, the background (water and sea ice) is described by a statistical distribution. The data is assigned to the background if it is consistent with the distribution; otherwise it is identified as a target. The threshold for the detection of targets is controlled by the calculated statistical probability that the detection is false. The threshold is adjusted to maintain a constant ‘false alarm rate’ in the resulting product [Gill, 2001].

Automatic algorithms are known to have errors, so a target identified in both the PMR and CFAR product is considered by the analyst to be a real physical target—most likely an iceberg. These methods give no information on the size of the targets, but the methods have proven to be very useful operationally for estimating populations and densities of icebergs.

Icebergs are common everywhere in Greenland waters and operational information on the presence of icebergs is an important parameter for safe navigation. However, the number of icebergs is very large, especially in eastern Baffin Bay between Disko Bay and Cape York. Here, more than 20 wide glacial outlets produce more than 10,000 icebergs every year. Some icebergs may be up to 1 km in length, but the majority of offshore icebergs are smaller, typically a few hundred meters in length. Near the shore, many icebergs frequently become grounded and are accompanied by large belts of bergy bits (5 m to 15 m) and growlers (< 5 m).

Icebergs near Greenland are mapped using the World Meteorological Organization’s Sea-Ice Nomenclature [WMO Pub No 259 TP. 145, excerpted in the ice chart symbology section at the end of this chapter]. The information on the distribution of icebergs is given in terms of *few* or *many* icebergs or growlers. In case of a large amount of glacial ice in an area, the “egg code” is used in the same way as it is for sea ice. For safety reasons, even ice-strengthened vessels are normally advised to avoid iceberg areas.

The case study below shows the RADARSAT-1 products used by the ice analyst and the resulting ice chart for eastern Baffin Bay for 27 July 2001 (Figures 20.15 to 20.18). It is very important for the ice analyst to be familiar with the normal ice conditions in the area in order to map all ice features relevant for safe navigation. This example applies to the operational DMI scenario and focuses on the phases of ice chart production for Eastern Baffin Bay (75°N, 60°W), with first-year-medium sea ice and many icebergs.



Figure 20.15. Typical photo from Eastern Baffin Bay (near 75°30N, 59°W), 8 September 1997. Many icebergs, bergy bits and growlers characterize the shore region in this area. Background information is very important for an ice analyst to interpret available satellite data correctly. (Photo: Keld Q. Hansen, DMI)

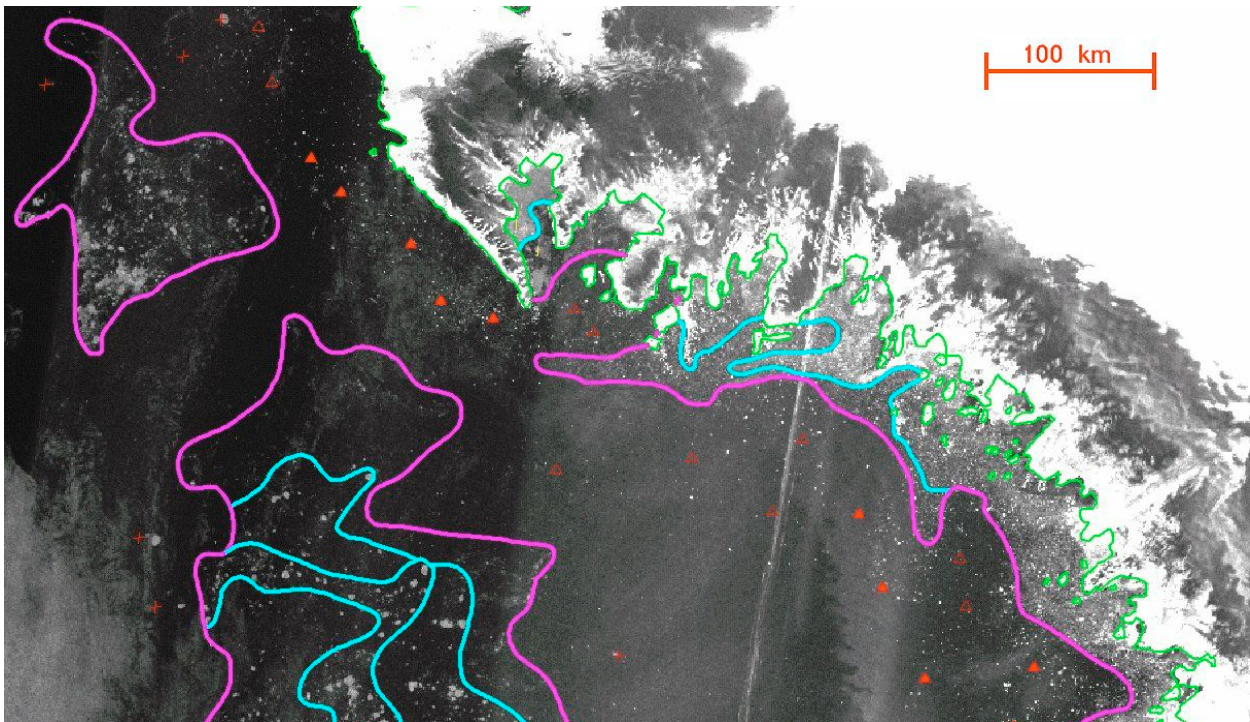


Figure 20.16. Ascending RADARSAT-1 (C-band, HH) ScanSAR-Wide image, 27 July 2001, 2130 UTC received and analyzed operationally at the Danish Meteorological Institute. The ice polygon boundaries as interpreted by the ice analyst are overlaid. The image contains large icebergs, relatively large sea ice floes (left), and wide belts of icebergs, bergy bits, and growlers (near the shore). ©CSA 2001

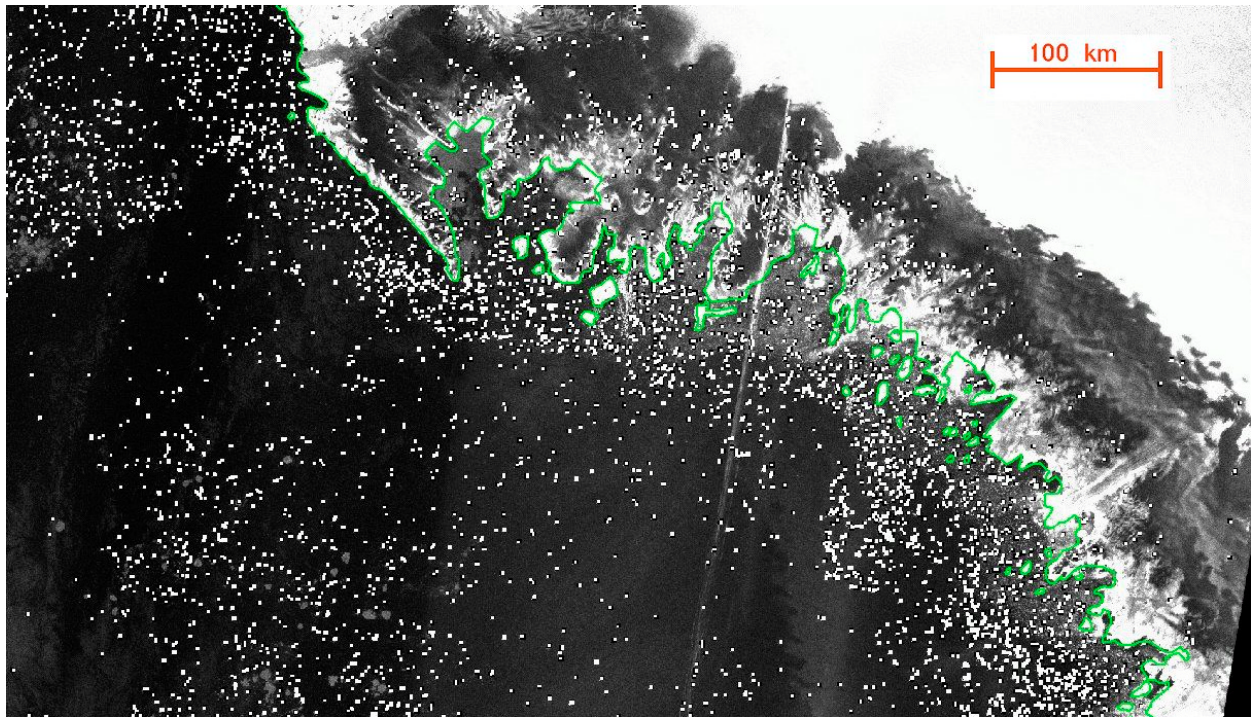


Figure 20.17. The CFAR (Constant False Alarm Rate) detection algorithm applied to the RADARSAT-1 image in Figure 20.16. The CFAR algorithm is used in combination with the Power-to-Mean filter to enhance information about the number of targets at the sea surface.

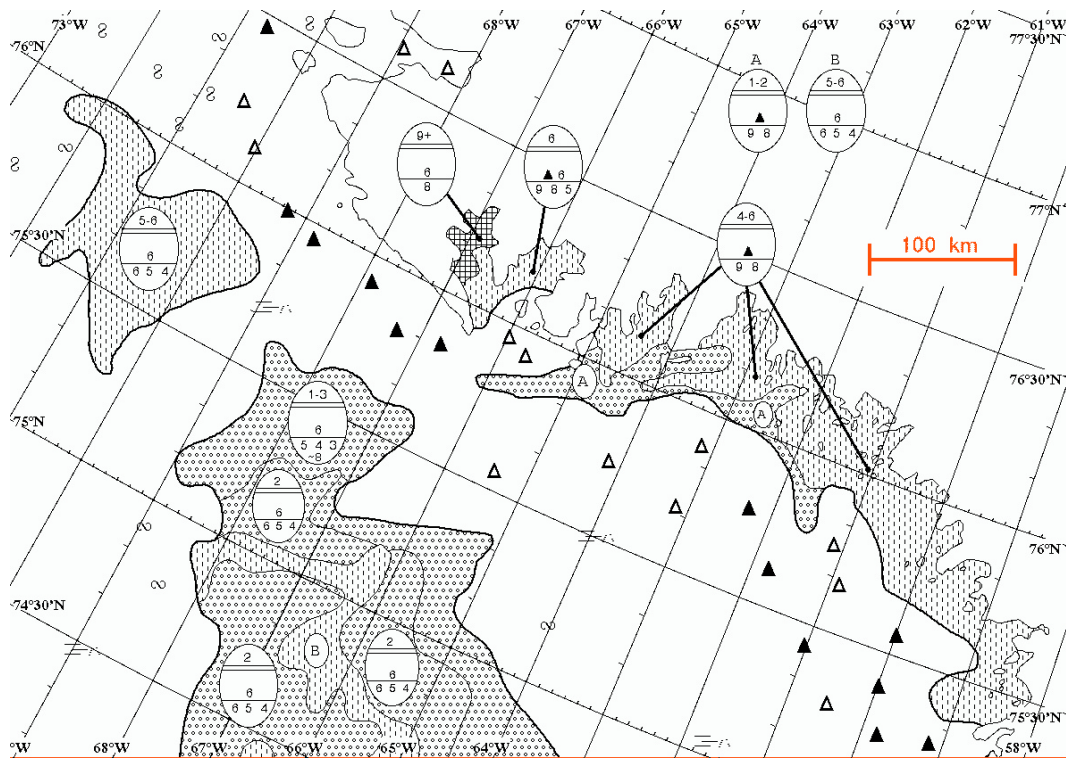


Figure 20.18. Resulting ice chart from the interpretation of Figures 20.16 and 20.17. The ice polygons have been formatted cartographically and the WMO ice egg code symbols (see the ice chart symbology section at the end of the chapter) added. The presence and distribution of icebergs is represented by the triangular symbols.

20.3.5 *National Ice Center and Canadian Ice Service:  
Great Lakes Analysis 22 February 2001*

This case study highlights the shared responsibility between the U.S. and Canada for ice charting in the Great Lakes. The lakes are an area of common operational interest; the collection of satellite imagery and the production of charts is coordinated between the two ice centers. The NIC issues a chart of all five Great Lakes weekly and also issues the CIS-produced, five-lake composite weekly. The CIS issues daily charts of a subset of lakes as required to support navigation and also issues the NIC-generated composite chart weekly. Both ice services share satellite data sets and analyses for the generation of their respective products.

In Figure 20.19, high concentrations of ice are evident in Lake Erie. The ice concentration, ice deformation, and, therefore, ice thickness increase towards the eastern end of Lake Erie under the influence of seasonally-predominant westerly winds that funnel the ice into the narrower eastern end of the lake. The bright returns seen in this area indicate strong deformation conditions. Low ice concentration, thinner ice types, and less deformed ice are present in the western portion of the lake, which is typically an area of new ice formation. Wind conditions at the time of the image acquisition were southwest at 5 to 8 m s<sup>-1</sup>, and the temperatures ranged from -8°C to -5°C. Because the Great Lakes are fresh water, the ice signatures differ from those for sea ice and are driven by a combination of both surface and volume scattering in all ice thickness types.

In Lake Huron, low to moderate concentrations of ice are evident around the southwestern and southeastern shores. Higher concentrations and thickness types are evident in the Saginaw Bay and along the northeastern shores because of their shallow depth and relatively sheltered topography. A large area of open water is clearly visible in the central portion of the lake. The high return of the younger ice types in the southern portion of the lake result from the predominant westerly wind compacting ice along the eastern shoreline, creating fields of brash ice. Brash ice (small floes of different ice types that result from collisions within the ice pack) has highly angular topography and consequently bright returns in SAR imagery. At the time of the image, the winds were from the south at 2 to 5 m s<sup>-1</sup> and sections of brash ice are visible drifting away from the southern coastline.

In the small sections of Lakes Superior and Michigan covered by the SAR swath, ice is located only along the eastern margins. It is interesting to note the relatively high backscatter in these two lakes over open water (compared to the other lakes) as a result of imaging at small incident angles (20° to 35°) in the near range of the ScanSAR imagery. Again, predominant westerly winds have compacted the ice along the eastern shores. In northeastern Lake Michigan, the inset sub-image shows a bright linear feature between the open water and the area of ice packed into the Straits of Mackinac. This feature is a typical signature in SAR imagery that indicates that ice is under compaction. A linear region of high return results from the interaction of the wind and waves with the ice pack. This interaction causes ice to pile up along the ice edge. This bright linear feature is very useful in edge identification. A similar signature can be seen where fast ice boundaries interact with open water or pack ice areas.

Ice charts resulting from the analysis of this RADARSAT-1 scene and other data sources are presented in Figures 20.20a and 20.20b.

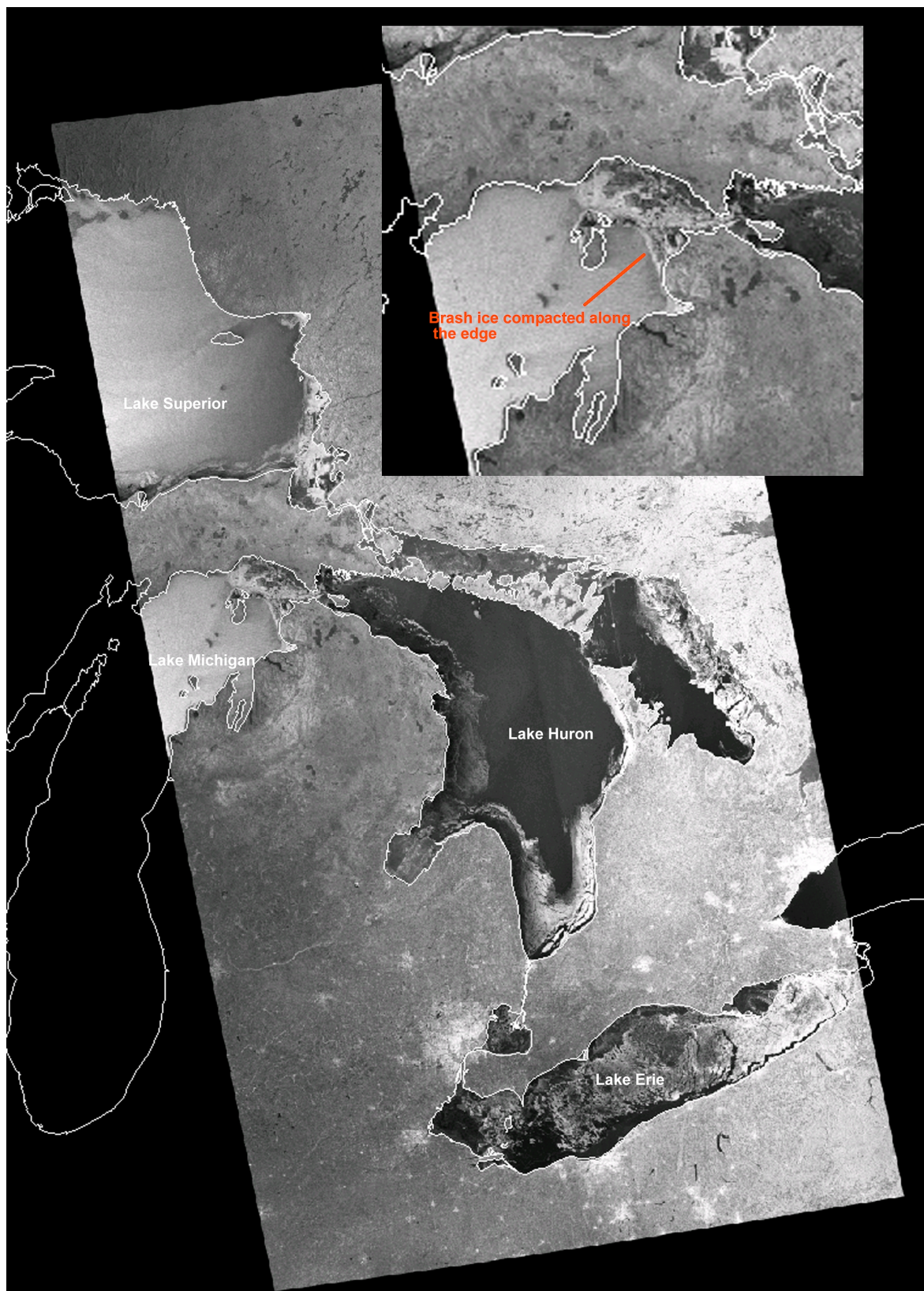


Figure 20.19. A RADARSAT-1 (C-band, HH) ScanSAR Wide-A swath covering the central Great Lakes, acquired 22 February 2001 at 2333 UTC. ©CSA 2001

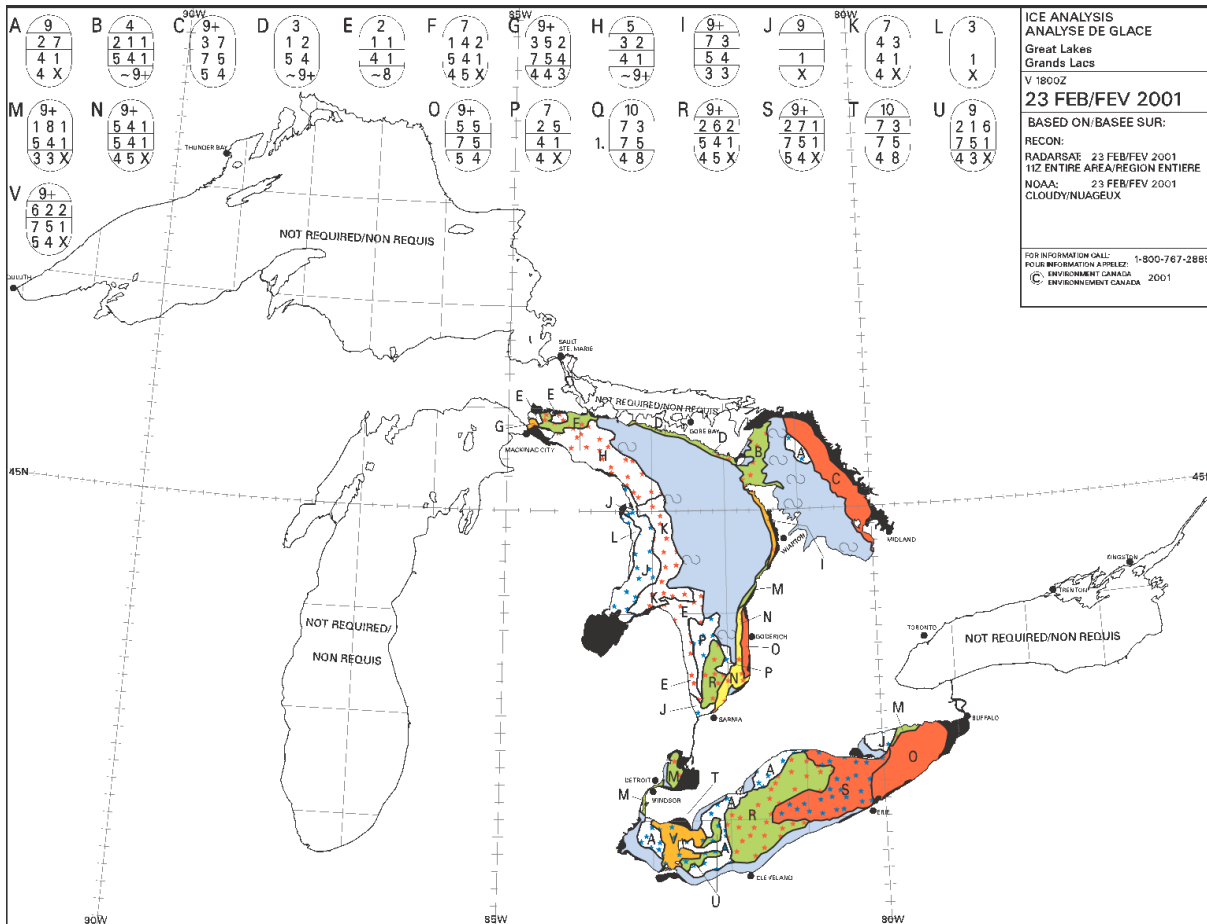


Figure 20.20a. Canadian Ice Service Great Lakes daily chart, based on image in Figure 20.19.

## 20.4 Outlook

The mandate of the U.S., Canadian, and Danish ice centers is to provide accurate and timely information about ice conditions, primarily for safety of navigation. Information about ice conditions is extracted from a wide range of satellite data sources combined with supporting meteorological and oceanographic data and the experience of skilled ice analysts.

In a digital workstation environment, ice analysts have the ability to enhance, combine, and animate imagery to perform a manual assimilation of all available data, including sea ice climatology, meteorological charts, and imagery from visible, infrared, and passive microwave sensors. Iceberg mapping is assisted using automated techniques to highlight point targets and ice edge information. In order to map the Arctic, an ice center's analysts may view many gigabytes of satellite imagery on a daily basis.

As long as SAR imagery has been routinely available, ice centers have successfully used it to produce ice maps in support of safety of navigation. Accurate ice analyses and forecasts depend heavily on the availability of the all-weather, high spatial resolution, wide swath capabilities of satellite SAR. SAR increases the spatial accuracy of ice charts and permits better distinction of ice types and navigation hazards such as ridging. SAR is the only satellite data source suitable for operationally mapping ice conditions at a tactical navigation scale. Currently, at the U.S. National Ice Center, 23% of all Northern Hemisphere analysis lines can be directly

SAR for Operational Ice Observation and Analysis

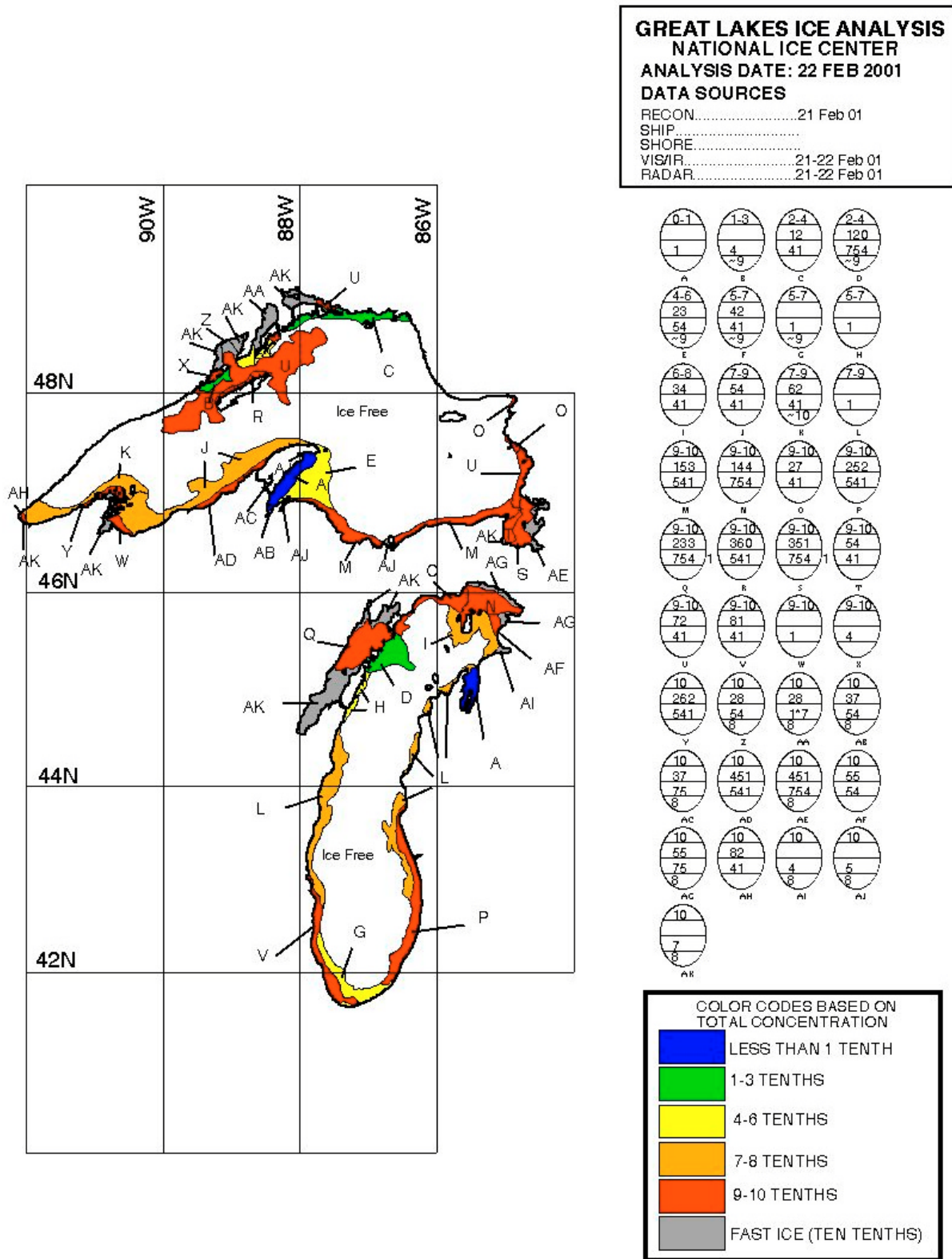


Figure 20.20b. NIC Western Great Lakes weekly composite based on imagery acquired immediately prior to the images shown in Figure 20.19. This chart nicely complements Figure 20.20a, giving mariners a complete picture of ice navigation conditions in the lakes.

attributed to SAR imagery, and over 50% of Alaska/Great Lakes analysis lines are drawn from SAR data. These numbers would be much larger if SAR data were available over the entire area that is mapped weekly. At the Canadian and Danish ice services, it is estimated that between 80% and 90% of analysis lines are attributed to satellite SAR imagery.

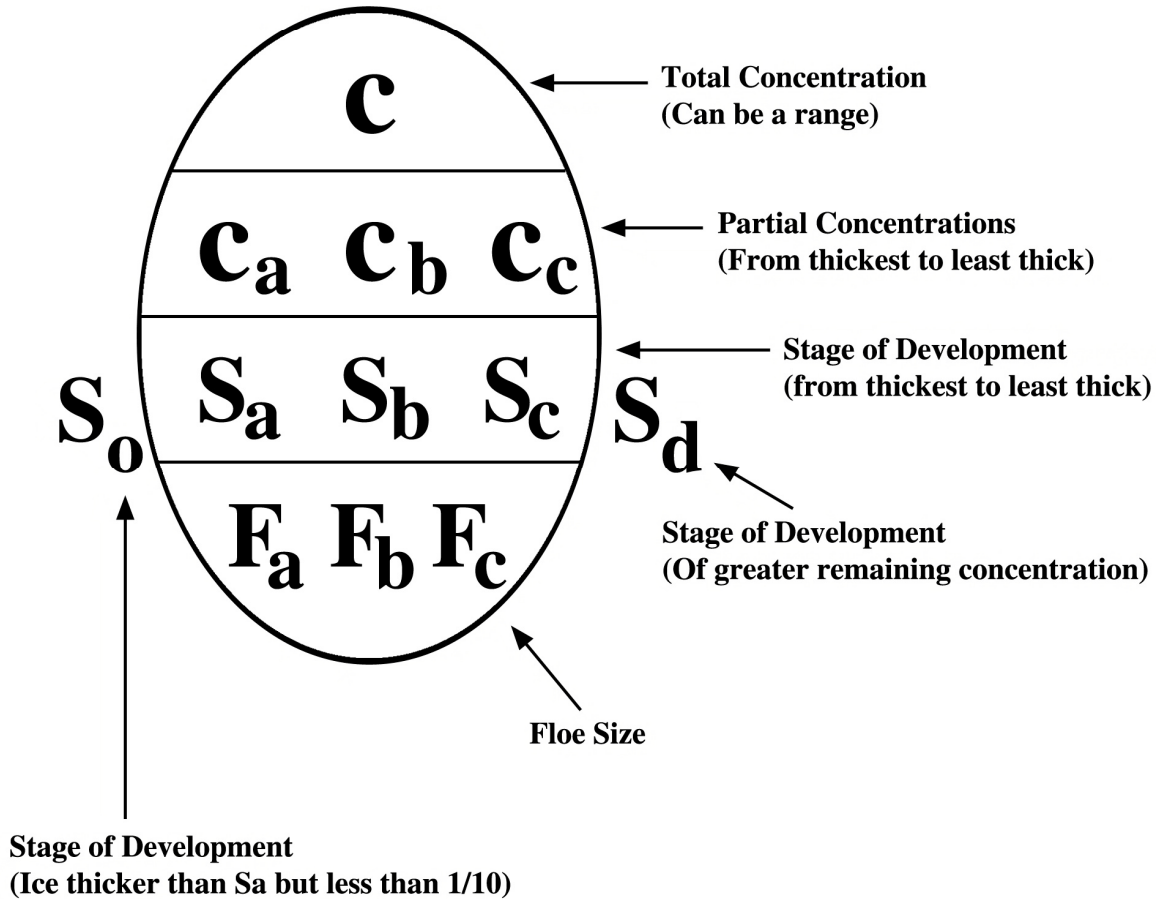
The increase in the use of SAR has led to dramatic changes of the operational procedures at the ice centers; considerable resources have been allocated to SAR-related training of ice analysts and quality assurance programs. Research and development to optimize the use of SAR data has intensified, new computer-based analysis systems have been developed to facilitate effective assimilation of many different data sources, and economic resources have been relocated from conventional aerial ice reconnaissance to SAR image acquisition.

Determination of the ice/water boundary and ice types under summer melt conditions remains problematic; thus, the ice centers continue to use SAR imagery in conjunction with other data sources during the summer season. Because manual analysis techniques remain the primary mode of operational analysis, ice centers have been largely unaffected by the unavailability of calibrated data in near-real-time. Development continues on automated information extraction techniques, (including improved image segmentation, data fusion, and expert-system approaches – e.g., *Bertoia et al.*, 1998, 1999; *Soh and Tsatsoulis*, 1999; *Clausi*, 2001, 2002) which have so far not met operational requirements for timeliness and accuracy. One example of an automated extraction approach using current data is the RADARSAT Geophysical Processor System [*Kwok and Balzer*, 1995], which uses the frequent revisit capability of wide-swath SAR to track ice motion and estimate ice thickness. However, this system operates in a research mode and does not meet the near-real-time requirements of the operational ice centers. The availability of multi-polarization and polarimetric SAR from future satellites (e.g., ENVISAT, RADARSAT-2, PALSAR) is expected to improve the information content of the imagery and may provide greater opportunities for operational automation [*Nghiem and Bertoia*, 2001].

The capabilities of future operational SAR satellites will enhance and improve the use of SAR products for ice charting. Recently, the European satellite ENVISAT has been successfully launched and it is foreseen that images from its Advanced Synthetic Aperture Radar, in combination with images from RADARSAT-1 and later RADARSAT-2, will be the ice centers' principal information source. Furthermore, it is expected that the new SAR modes becoming available will provide new ways to extract information about ice conditions, including (semi)-automatic extraction of certain sea ice parameters. The ice centers therefore look forward to a robust constellation of future SAR satellites for continued reliable production of regional and global sea ice charts.

## ICE CHART SYMBOLOGY - EGG CODE

The World Meteorology Organization (WMO) system for sea ice symbology is more frequently referred to as the "Egg Code" due to the oval shape of the symbol. A brief description of the code follows.



### Total Concentration

The total concentration (C) of ice in area, reported in tenths and is the uppermost group. Concentration may be expressed as a single number or as a range, not to exceed two tenths (3-5, 5-7 etc.)

### Partial Concentration

Partial concentration (C<sub>a</sub>, C<sub>b</sub>, C<sub>c</sub>) are reported in tenths, but must be reported as a single digit. These are reported in order of decreasing thickness. C<sub>a</sub> is the concentration of the thickest ice and C<sub>c</sub> is the concentration of the thinnest ice.

### Stages of Development

Stages of development (S<sub>a</sub>, S<sub>b</sub>, S<sub>c</sub>) are listed using the following code in decreasing order of thickness. These codes are directly correlated with the partial concentrations above. C<sub>a</sub> is the concentration of stage S<sub>a</sub>, C<sub>b</sub> is the concentration of stage S<sub>b</sub>, and C<sub>c</sub> is the concentration of S<sub>c</sub>. S<sub>o</sub> if reported is a trace of ice type thicker/older than S<sub>a</sub>. S<sub>d</sub> is a thinner ice type which is reported when there are four or more ice thickness types. (Table 1)

### Forms of Ice

Predominant form (F<sub>a</sub> F<sub>b</sub> F<sub>c</sub>) of ice (floe size) corresponding to S<sub>a</sub>, S<sub>b</sub> and S<sub>c</sub> respectively. (Table 2)

Table 1 Codes for Ice Stages of Development

<i>The following codes are used to denote stages of development for sea ice.</i>		<i>The following codes are used to denote stages of development for fresh water ice:</i>	
Stage of Development	Code Figure	Stage of Development	Code Figure
New Ice-Frazil, Grease, Slush, Shuga (0-10 cm)	1	New Ice (0 cm - 5 cm)	1
Nilas, Ice Rind (0-10 cm)	2	Thin Ice (5 cm - 15 cm)	4
Young (10-30 cm)	3	Medium Ice (15 cm - 30 cm)	5
Gray (10-15 cm)	4	Thick Ice (30 cm - 70 cm)	7
Gray-White (15-30 cm)	5	First Stage Thick Ice (30 cm - 50 cm)	8
First Year (30-120 cm)	6	Second Stage Thick Ice (50 cm - 70 cm)	9
First Year Thin (30-70 cm)	7	Very Thick Ice (70 cm - 120 cm)	1.
First Year Thin- First Stage (30-70 cm)	8		
First Year Thin- Second Stage (30-70 cm)	9		
Med First Year (70-120 cm)	1.		
Thick First Year (>120 cm)	4.		
Old-Survived at least one seasons melt (>2 m)	7.		
Second Year (>2 m)	8.		
Multi-Year (>2 m)	9.		
Ice of Land Origin	▲		

Table 2. Codes for Forms of Ice

<i>The following codes are used to denote forms of sea ice:</i>		<i>The following codes are used to denote forms of sea ice for fresh water ice:</i>	
Forms of Sea Ice	Code Figure	Forms of Sea Ice	Code Figure
New Ice (0 cm - 10 cm)	X	Fast Ice	8
Pancake Ice (30 cm - 3 m)	0	Belts and Strips symbol followed by the concentration of ice	~F
Brash Ice (less than 2 m)	1		
Ice Cake (3 m - 20 m)	2		
Small Ice Floe (20 m - 100 m)	3		
Medium Ice Floe (100 m - 500 m)	4		
Big Ice Floe (500 m - 2 km)	5		
Vast Ice Floe (2 km - 10 km)	6		
Giant Ice Floe (greater than 10 km)	7		
Fast Ice	8		
Ice of Land Origin	9		
Undetermined or Unknown (Iceberg, Growlers, Bergy Bits) (Used for Fa, Fb, Fc, only)	/		

## 20.5 References

- Bertoia, Cheryl and J. Falkingham, F.Fetterer, 1998. Polar SAR Data for Operational Sea Ice Mapping, in R. Kwok and C. Tsatsoulis (Eds.). *Recent Advances in the Analysis of SAR Data of the Polar Oceans*, Springer Verlag: Berlin, pp. 201-234.
- Bertoia, C., D. Gineris, K. Partington, L.-K. Soh and C. Tsatsoulis, 1999. "Transition from research to operations: ARKTOS: A knowledge-based sea ice classification system," in Proc. IGARSS'99, Hamburg, Germany, pp. 1573-1574.
- Canadian Ice Service, 2001. *Annual Arctic Ice Atlas*,. Environment Canada, Ottawa (annual publication), ISBN 0-662-65773-X.
- Clausi, D.A., 2002. An analysis of co-occurrence texture statistics as a function of grey level quantization. *Canadian Journal of Remote Sensing*, Vol. 28, No. 1, pp. 45-62.
- Clausi, D.A., 2001. Comparison and fusion of co-occurrence, Gabor, and MRF texture features for classification of SAR sea ice imagery. *Atmosphere-Ocean, NOW Special Issue*, Vol. 39, No. 4, pp. 183-194.
- Gill, R. S., 2001. "Operational Detection of Sea Ice Edges and Icebergs Using SAR." *Canadian Journal of Remote Sensing*, Vol. 27, no. 5, pp. 411-432.
- Gill, R. S., and H.H. Valeur, P. Nielsen, 1997. "Evaluation of the Radarsat images in the operational mapping of the sea ice in the Greenland waters", in the *Geomatics in the Year of Radarsat, GER'97 symposium*, Ottawa, May.
- Gill, R.S., and M. K. Rosengreen, H. Valeur, 2000. "Operational Ice Mapping with RADARSAT for Ship Navigation in the Greenland Waters." *Canadian Journal of Remote Sensing*, Vol 26, No. 2, p121 – 132.
- Kwok, R. and T. Balzer, 1995. The Geophysical Processor System at the Alaska SAR Facility. *Photogramm. Engrg. And Remote Sensing*, Vol. 61, No. 12, pp. 1445-1453.
- Nghiem, Son and C. Bertoia, 2001. Study of Multi-Polarization C-Band Backscatter Signatures for Arctic Sea Ice Mapping with Future Satellite SAR. *Canadian Journal of Remote Sensing*, Vol. 27, No. 5, pp. 387-402.
- Ramsay, B., D. Flett, M. Manore, R. De Abreu, 2001. RADARSAT-1 for Sea Ice Monitoring In Canada. *Proceedings IGARSS'01, Sydney, Australia, July 2001*.
- Soh, L.-K. and C. Tsatsoulis, 1999. "Multisource data and knowledge fusion for intelligent SAR sea ice classification," in Proc. IGARSS'99, Hamburg, Germany, 1999, pp. 68-70.
- Soh, L.-K. and C. Tsatsoulis, 1999. Unsupervised segmentation of ERS and Radarsat sea ice images using multiresolution peak detection and aggregated population equalization. *Int. J. Remote Sensing*, Vol. 20, No. 15 &16, pp. 3087-3109.

## 20.6 Related Articles

- Bertoia, C., and B. Ramsay, 1998: Sea ice analysis and products: Cooperative work at the U.S. and Canadian National Ice Centers. *Proc. 1998 Int. Geoscience and Remote Sensing Symp.*, Seattle, WA, IEEE, 1944–1947.
- , D. Gineris, K. Partington, L. K. Soh, and C. Costas Tsatsoulis, 1999: Transition from research to operations: ARKTOS—A knowledge-based sea ice classification system. *Proc. 1999 Int. Geoscience and Remote Sensing Symp.*, Hamburg, Germany, IEEE, 1573–1574.
- Canadian Ice Service, 2002: MANICE: Manual of standard procedures for observing and reporting ice conditions. 9th ed. Environment Canada, ISBN 0-660-61977-6, 130 pp.

- Dedrick, K. R., K. Partington, M. Van Woert, C. A. Bertoia, and D. Benner, 2001: U.S. National/Naval Ice Center digital sea ice data and climatology. *Can. J. Remote Sens.*, **27**, 5, 457–475.
- Gill, R., and H. H. Valeur, 1996: Evaluation of the RADARSAT imagery for the operational mapping of sea ice around Greenland. Danish Meteorological Institute Scientific Rep. 96-9, 98 pp.
- Leshkevich, G., W. Pichel, P. Clemente-Colon, R. Carey, and G. Hufford, 1995: Analysis of coastal ice cover using ERS-1 SAR data. *Int. J. Remote Sens.*, **16**, 3459–3479.
- Shuchman, R., C. Wackerman, and L. Sutherland, 1991: The use of synthetic aperture radar to map the Polar Oceans. ERIM Technical Manual, 333 pp.
- United States Hydrographic Office, 1952: A functional glossary of ice terminology. U.S. Navy Hydrographic Office Publ. 609, Washington, DC, 88 pp.
- Winebrenner, D. P., L. D. Farmer, and I. R. Joughin, 1995: On the response of polarimetric synthetic aperture radar signatures at 24-cm wavelength to sea ice thickness in Arctic leads. *Radio Sci.*, **30**, 373–402.
- WMO, 1970: WMO Sea-Ice Nomenclature. WMO 259, TP 145, Secretariat of the World Meteorological Organization, 147 pp.